

# Input output linearization on the H-drive including tilt of the beam

**Citation for published version (APA):**

Wouters, R. M. T., & Nijmeijer, H. (2004). *Input output linearization on the H-drive including tilt of the beam*. (DCT rapporten; Vol. 2004.037). Technische Universiteit Eindhoven.

**Document status and date:**

Published: 01/01/2004

**Document Version:**

Publisher's PDF, also known as Version of Record (includes final page, issue and volume numbers)

**Please check the document version of this publication:**

- A submitted manuscript is the version of the article upon submission and before peer-review. There can be important differences between the submitted version and the official published version of record. People interested in the research are advised to contact the author for the final version of the publication, or visit the DOI to the publisher's website.
- The final author version and the galley proof are versions of the publication after peer review.
- The final published version features the final layout of the paper including the volume, issue and page numbers.

[Link to publication](#)

**General rights**

Copyright and moral rights for the publications made accessible in the public portal are retained by the authors and/or other copyright owners and it is a condition of accessing publications that users recognise and abide by the legal requirements associated with these rights.

- Users may download and print one copy of any publication from the public portal for the purpose of private study or research.
- You may not further distribute the material or use it for any profit-making activity or commercial gain
- You may freely distribute the URL identifying the publication in the public portal.

If the publication is distributed under the terms of Article 25fa of the Dutch Copyright Act, indicated by the "Taverne" license above, please follow below link for the End User Agreement:

[www.tue.nl/taverne](http://www.tue.nl/taverne)

**Take down policy**

If you believe that this document breaches copyright please contact us at:

[openaccess@tue.nl](mailto:openaccess@tue.nl)

providing details and we will investigate your claim.

Input output linearization on the  
H-drive including tilt of the beam

R.M.T. Wouters

DCT.2004.37

Report internship

Coach: Prof.dr. H. Nijmeijer

EINDHOVEN UNIVERSITY OF TECHNOLOGY  
DEPARTMENT OF MECHANICAL ENGINEERING  
DYNAMICS AND CONTROL GROUP

Eindhoven, March 15, 2004

# Summary

In the Dynamics and Control Technology laboratory of the Department of Mechanical Engineering a so called H-drive servo system is used for experimenting with different types of controllers. The H-drive servo system is an XY-table with three linear motors that has been build by Philips' Centre for Industrial Technology (CIT) as part of an Advanced Component Mounter (ACM) for pick-and-place operations on printed circuit boards.

In this report a controller is designed which makes stabilization and tracking of the x- and y-position of the X-motor possible. An extra feature of the controller is the tilt stabilization of the beam on which the X-motor is mounted. The controller consists of a high- and low-level controller. The high-level controller provides a reference trajectory while the low-level controller generates the desired current to the linear motors. The advantage of this control structure is the possibility to suppress cogging and friction forces.

The high level controller uses an input output linearization technique to make the output (motor positions) linear to the input of a tracking controller. Because of the H-drive model nature it appears that controlling the H-drive is possible when the input output linearization provides a value for the desired acceleration. By integrating the desired acceleration twice a reference trajectory can be generated. The low level controller generates a current using the difference between the real trajectory and the trajectory generated by the high level controller. The used low-level controller consists of three PID-controllers and is designed in a report of Aart-Jan van der Voort.

To check the validity of the designed controller a simulation program is made. In this simulation program the X-LiMMS has to follow a certain trajectory. The chosen trajectory makes verification of the stabilizing and tracking performance of the controller possible. The simulation and experimental results correspond well but the output of the controller (currents) shows a noisy behavior of the experiment. The applied currents during the experiment are also significantly larger than the simulated ones. This is probably caused by the friction and cogging forces in the H-drive. To improve the experimental results a feedforward amplification is introduced which results in a significant reduction of the tracking error.

# Contents

Summary	i
<b>1 Introduction</b>	<b>1</b>
<b>2 Equations of motion</b>	<b>3</b>
<b>3 Input output linearization</b>	<b>6</b>
<b>4 Controller design</b>	<b>9</b>
4.1 Control strategy . . . . .	9
4.2 IO controller . . . . .	10
<b>5 Simulations and Experiments</b>	<b>12</b>
5.1 Reference trajectory . . . . .	12
5.2 Parameters . . . . .	14
5.3 Simulation results . . . . .	14
5.4 Experimental results . . . . .	16
<b>6 Conclusions and Recommendations</b>	<b>20</b>
6.1 Conclusions . . . . .	20
6.2 Recommendations . . . . .	21
<b>A Results of the Lagrange equations of motion</b>	<b>22</b>
A.1 Kinetic energy . . . . .	22
A.2 Lagrange equations of motion . . . . .	22

<i>Contents</i>	iii
<b>B Results of the IO linearization</b>	<b>24</b>
B.1 The matrix $A(x)$ and vector $N(x)$ . . . . .	24
B.2 Non-singularity proof $A(x)$ . . . . .	26
B.3 The state feedback law . . . . .	28
<b>C IO linearization using matrix/vector calculation</b>	<b>29</b>
<b>D Experiment with feedforward amplification</b>	<b>31</b>
<b>E Programs used for the simulation and experiment</b>	<b>34</b>
<b>Bibliography</b>	<b>35</b>

# Chapter 1

## Introduction

Within the section Dynamics and Control of the Department Mechanical Engineering research is done on controllability of underactuated systems. These systems contain more degrees of freedom than inputs. A teststand that is used for research on this subject is an adjusted H-drive. This H-drive is an XY-table with three linear motors i.e. Linear Motion Motor Systems (LiMMS). The two Y-LiMMS, which move parallel, are connected by a beam on which the X-LiMMS can move. On top of the X-LiMMS an extra degree of freedom is installed in the form of an unactuated pendulum that can rotate freely in the horizontal plane.

To reduce complexity of the mathematical models, that are used for previous development of controllers, the assumption was made that the Y-LiMMS and the beam behave like one rigid body. This means that the angle between the Y-guideway and beam is assumed to be always 90 degrees. The two Y-LiMMS can then be modelled like one LiMMS.

Practically the Y-LiMMS and the beam are not constructed as one rigid body. The beam is connected to the Y-LiMMS by two joints, which allow a small rotation in the horizontal plane. That this system has a different dynamical behavior than the models assuming rigid body behavior of the Y-LiMMS and the beam can be explained by the following example. Presume an eccentric load on the beam, caused by the X-LiMMS, and that the angle between the beam and the Y-guide must remain 90 degrees. It is obvious that in this situation the nearest Y-LiMMS provides more force than the furthest Y-LiMMS. If both Y-LiMMS would provide an equal force, like models assuming rigid body behavior of the Y-LiMMS and the beam, the beam would tilt.

This report is written within the scope of an internship where research is done on the controllability of the H-drive including tilt of the beam. The designed controller makes use of input output linearization and offers the possibility to stabilize the tilt of the beam.

Chapter 2 of this report discusses the determination of the nonlinear H-drive model

which includes the tilt of the beam. In chapter 3 the input output linearization of the H-drive model is discussed. The aim of this linearization is to make the H-drive input (current to the LiMMS) linear to the H-drive outputs. The outputs of the H-drive will be defined as the x- and y-position of the X-LiMMS and the tilt of the beam. The control strategy which will be discussed in section 4.1 employs a high and low level controller. The construction of the high level controller which makes use of the input output linearization and a tracking controller is explained in section 4.2. By integrating the result of the high level controller twice a reference trajectory for the low level controller can be generated. The low level controller which consists of three PI lead/Lag controllers in series with a second-order low-pass generates an appropriate value for the currents to the LiMMS. In chapter 5 the results of a simulation and experiment will be presented. In the last chapter conclusions and recommendations are made.

## Chapter 2

# Equations of motion

In this chapter the equations of motion are derived using Lagrange equations according to [7]. The dynamic model of the H-drive used to derive these equations is shown in figure 2.1. It consists of two parallel Y-axes that are connected by a beam, the X-axis.

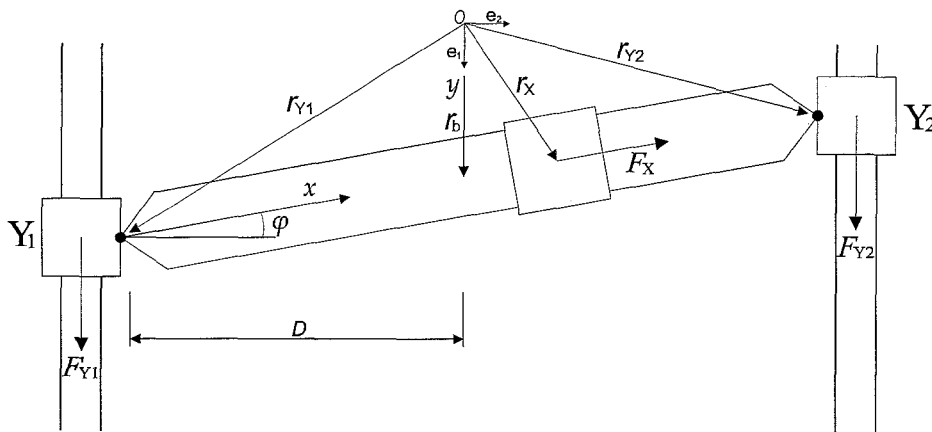


Figure 2.1: Schematic representation of the H-drive with generalized coordinates  $\underline{q} = [y, \varphi, x]^T$ . source:[4]

The beam, or X-axis, is connected to the Y-axes by two joints that allow rotations in the horizontal plane. Therefore the positions Y1 and Y2 do not need to be equal which can cause a tilt of the X-axis. The position of the beam along the X-axis and Y-axes is controlled by three Linear Motion Motors Systems (LiMMS). Each linear motor has its own servo system, encoder sensors and is current-controlled. The position of the three LiMMS, and the beam can be written in the absolute coordinates  $\vec{e} = [\vec{e}_1, \vec{e}_2]^T$ . For the



dynamic model depicted in figure 2.1 this results in;

$$\begin{aligned} \vec{r}_b &= \begin{bmatrix} y \\ 0 \end{bmatrix} \vec{e} \quad , \quad \vec{r}_X = \vec{r}_{Y1} + x \begin{bmatrix} -\sin(\varphi) \\ \cos(\varphi) \end{bmatrix} \vec{e} \\ \vec{r}_{Y1} &= \vec{r}_b + D \begin{bmatrix} \tan(\varphi) \\ -1 \end{bmatrix} \vec{e} \quad , \quad \vec{r}_{Y2} = \vec{r}_b + D \begin{bmatrix} -\tan(\varphi) \\ 1 \end{bmatrix} \vec{e} \end{aligned} \quad (2.1)$$

in which  $\vec{r}_b$ ,  $\vec{r}_X$ ,  $\vec{r}_{Y1}$  and  $\vec{r}_{Y2}$  are the position vectors of the beam, X-LiMMS, Y1- LiMMS and Y2-LiMMS respectively. To indicate these positions the generalized coordinate system  $[y, \varphi, x]$  is used. Note that the origin of the absolute coordinate system is located in the middle of the Y1 and Y2 guide. The distance from the guides to the origin is denoted by  $D$ .

The inputs of the system, the LiMMS currents, are given by  $\underline{u} = [i_{Y1}, i_{Y2}, i_X]^T$ . The forces generated by the LiMMS can then be written as

$$\begin{aligned} \vec{F}_{Y1} &= \begin{bmatrix} k_m i_{Y1} \\ 0 \end{bmatrix} \vec{e} \quad , \quad \vec{F}_{Y2} = \begin{bmatrix} k_m i_{Y2} \\ 0 \end{bmatrix} \vec{e} \\ \vec{F}_X &= \begin{bmatrix} -k_m i_X \sin(\varphi) \\ k_m i_X \cos(\varphi) \end{bmatrix} \vec{e} \end{aligned} \quad (2.2)$$

where  $k_m$  represents the motor constant of the LiMMS. Here it is assumed that all LiMMS have an equal motor constant.

The outputs of the system are defined as:

$$\begin{aligned} y_1 &= y + D \tan(\varphi) - x \sin(\varphi) \\ y_2 &= \varphi \\ y_3 &= -D + x \cos(\varphi) \end{aligned} \quad (2.3)$$

Output  $y_1$  represents the position of the X-LiMMS in the  $\vec{e}_1$  direction. The second output indicates the angle of the beam. The third output represents the position of the X-LiMMS in the  $\vec{e}_2$  direction.

With the masses of the beam, X-LiMMS, Y1-LiMMS and Y2-LiMMS which are respectively  $m_b$ ,  $m_X$ ,  $m_{Y1}$  and  $m_{Y2}$  the kinetic energy can be derived from:

$$T = \frac{1}{2} m_b \dot{\vec{r}}_b \cdot \dot{\vec{r}}_b + \frac{1}{2} m_X \dot{\vec{r}}_X \cdot \dot{\vec{r}}_X + \frac{1}{2} m_{Y1} \dot{\vec{r}}_{Y1} \cdot \dot{\vec{r}}_{Y1} + \frac{1}{2} m_{Y2} \dot{\vec{r}}_{Y2} \cdot \dot{\vec{r}}_{Y2} + \frac{1}{2} (J_b + J_x) \cdot \dot{\varphi}^2 \quad (2.4)$$

Due to the complexity of the resulting equation the kinetic energy will be written out in Appendix A.

When using the generalized coordinate system  $\underline{q} = [y, \varphi, x]^T$  the non-conservative forces can be derived from:

$$Q^{nc} = \sum_{i=1}^3 \left( \frac{\partial \vec{F}_i}{\partial \underline{q}} \right)^T \cdot \vec{F}_i \quad (2.5)$$

Using (2.5) the non-conservative forces (2.2) can be written as:

$$\underline{Q}^{nc} = k_m \begin{bmatrix} 1 & 1 & -\sin(\varphi) \\ D(1 + \tan(\varphi))^2 & -D(1 + \tan(\varphi))^2 & -D \sin(\varphi) / \cos^2(\varphi) \\ 0 & 0 & 1 \end{bmatrix} \begin{bmatrix} i_{Y1} \\ i_{Y2} \\ i_X \end{bmatrix} \quad (2.6)$$

Now the equations of motion can be derived using the Lagrange approach. The Lagrange equation of motion is given by:

$$\frac{d}{dt}(T, \underline{\dot{q}}) - T, \underline{q} + V, \underline{q} = (Q^{nc})^T \quad (2.7)$$

Here,  $T$  and  $Q^{nc}$  represent respectively the kinetic energy and the generalized non-conservative forces as obtained before. The vector  $V$  represents the potential energy which is not present in the H-drive model. Using matrix/vector notation the Lagrange equation can be rewritten in the form

$$\underline{M}(\underline{q})\underline{\ddot{q}} + \underline{C}(\underline{q}, \underline{\dot{q}})\underline{\dot{q}} + \underline{g}(\underline{q}) = \underline{\tau} \quad (2.8)$$

which simplifies a conversion to a first order differential equation. In this equation represents  $\underline{M}(\underline{q})$  the mass-matrix.  $\underline{C}(\underline{q}, \underline{\dot{q}})$  contains the coriolis and centripetal terms and  $\underline{g}(\underline{q})$  encompasses joint flexibility and gravitational effects. The vector  $\underline{\tau}$  represents the applied forces and torques, derived from  $\underline{Q}^{nc}$ .

When  $\underline{C}(\underline{q}, \underline{\dot{q}})\underline{\dot{q}}$  and  $\underline{g}(\underline{q})$  are combined in the term  $\underline{H}(\underline{q}, \underline{\dot{q}})$  and the vector  $\underline{\tau}$  is written as  $\underline{B}(\underline{q})\underline{u}$  then equation (2.8) takes the form of

$$\underline{M}(\underline{q})\underline{\ddot{q}} + \underline{H}(\underline{q}, \underline{\dot{q}}) = \underline{B}(\underline{q})\underline{u}. \quad (2.9)$$

In appendix A the matrices  $\underline{M}(\underline{q})$  and  $\underline{B}(\underline{q})$  and the vector  $\underline{H}(\underline{q}, \underline{\dot{q}})$  are given for the H-drive.

## Chapter 3

# Input output linearization

In this chapter input output linearization (IO-linearization), according to [5], will be applied on the H-drive model. A useful tool that will be used for this linearization is input output decoupling. Input output decoupling requires that, possibly after feedback, the  $i$ -th output is only influenced by the  $i$ -th input, and none of the other inputs.

To apply IO-linearization as described in [5], state space notation must be used. Using  $\underline{q} = [y, \varphi, x]^T$  the state will be defined as:

$$\underline{x} = \begin{bmatrix} \underline{x}_1 \\ \underline{x}_2 \end{bmatrix} = \begin{bmatrix} \underline{q} \\ \underline{\dot{q}} \end{bmatrix}. \quad (3.1)$$

Using

$$\dot{\underline{x}} = \underbrace{\begin{bmatrix} \underline{x}_2 \\ -M^{-1}(\underline{x}_1)H(\underline{x}_1, \underline{x}_2) \end{bmatrix}}_{f(x)} + \underbrace{\begin{bmatrix} 0 \\ M^{-1}(\underline{x}_1)B(\underline{x}_1) \end{bmatrix}}_{g(x)} \underline{u} \quad (3.2)$$

$$\begin{aligned} y_1 &= y + D \tan(\varphi) - x \sin(\varphi) \\ y_2 &= \varphi \\ y_3 &= -D + x \cos(\varphi) \end{aligned}$$

the equations of motion of the H-drive can be written in the form:

$$\begin{aligned} \dot{x} &= f(x) + g_1(x)u_1 + g_2(x)u_2 + g_3(x)u_3 \\ y_1 &= h_1(x) \\ y_2 &= h_2(x) \\ y_3 &= h_3(x). \end{aligned} \quad (3.3)$$

For Multi Input Multi Output (MIMO) systems of this form we can introduce the notion of relative degree with respect to each output. The definition is

$$y_j^{(\gamma_j)} = L_f^{\gamma_j} h_j + \sum_{i=1}^p L_{g_i} (L_f^{\gamma_j - 1} h_j) u_i \quad (3.4)$$

where  $\gamma_j$  is defined to be the smallest integer such that at least one of the inputs  $u_i$  appears in  $y_j^{(\gamma_j)}$ . For the H-drive the relative degree for each output equals 2 so:  $\gamma_1 = 2$ ,  $\gamma_2 = 2$  and  $\gamma_3 = 2$ . This can be easily verified because the inputs firstly appear in the second derivative of the generalized coordinates.

If the system has also well defined vector relative degree, then (3.4) can be written in the form

$$\begin{bmatrix} \ddot{y}_1 \\ \ddot{y}_2 \\ \ddot{y}_3 \end{bmatrix} = N(x) + A(x) \begin{bmatrix} u_1 \\ u_2 \\ u_3 \end{bmatrix} \quad (3.5)$$

where

$$N(x) = \begin{bmatrix} L_f^2 h_1 \\ L_f^2 h_2 \\ L_f^2 h_3 \end{bmatrix}, \quad A(x) = \begin{bmatrix} L_{g_1} L_f h_1 & L_{g_2} L_f h_1 & L_{g_3} L_f h_1 \\ L_{g_1} L_f h_2 & L_{g_2} L_f h_2 & L_{g_3} L_f h_2 \\ L_{g_1} L_f h_3 & L_{g_2} L_f h_3 & L_{g_3} L_f h_3 \end{bmatrix}. \quad (3.6)$$

The system has well defined vector relative degree  $\gamma_1, \gamma_2, \gamma_3$  at  $x$  if for all  $x$ :

$$L_{g_i} h_i(x) \equiv 0, \quad i = 1, 2, 3 \quad (3.7)$$

and the matrix  $A(x)$  is nonsingular.

Because the H-drive system satisfies (3.7) and  $A(x)$  is non-singular, see appendix B, a local state feedback control law

$$u = A^{-1}(x)(v - N(x)) \quad (3.8)$$

can be defined which yields the closed loop, decoupled, system

$$\begin{bmatrix} \ddot{y}_1 \\ \ddot{y}_2 \\ \ddot{y}_3 \end{bmatrix} = \begin{bmatrix} v_1 \\ v_2 \\ v_3 \end{bmatrix}. \quad (3.9)$$

For the H-drive the state feedback control law (3.8) is presented in Appendix B. This state feedback control law can also be obtained using matrix/vector calculation. The result of this method, which is the same as the previous method, is presented in Appendix C.

Next the system (3.3) can be written in a so called normal form. To do this we introduce a new coordinate system.

$$\begin{aligned} \xi_1^1 &= h_1(x), & \xi_2^1 &= L_f h_1(x), \\ \xi_1^2 &= h_2(x), & \xi_2^2 &= L_f h_2(x), \\ \xi_1^3 &= h_3(x), & \xi_2^3 &= L_f h_3(x). \end{aligned} \quad (3.10)$$

For the H-drive the preceding coordinate system can be written as:

$$\begin{aligned} \xi_1^1 &= y + D \tan(\varphi) - x \sin(\varphi), & \xi_2^1 &= \dot{y} + (D(1 + \tan^2(\varphi)) - x \cos(\varphi))\dot{\varphi} - \sin(\varphi)\dot{x} \\ \xi_1^2 &= \varphi, & \xi_2^2 &= \dot{\varphi} \\ \xi_1^3 &= -D + x \cos(\varphi), & \xi_2^3 &= -x \sin(\varphi)\dot{\varphi} + \cos(\varphi)\dot{x} \end{aligned} \quad (3.11)$$

The system equations, written in these coordinates have the following form

$$\begin{aligned}\dot{\xi}_1^1 &= \xi_2^1, \\ \dot{\xi}_2^1 &= v_1, \\ \dot{\xi}_1^2 &= \xi_2^2, \\ \dot{\xi}_2^2 &= v_2, \\ \dot{\xi}_1^3 &= \xi_2^3, \\ \dot{\xi}_2^3 &= v_3.\end{aligned}\tag{3.12}$$

The previous equations show that the outputs,  $\xi_1^1, \xi_1^2$  and  $\xi_1^3$  are decoupled w.r.t. the inputs,  $v_1, v_2$  and  $v_3$ . Observe that the system contains no zero or tracking dynamics.

Because  $\gamma_1 + \gamma_2 + \gamma_3 = 6$  equals the dimension of the system and  $A(x)$  has full rank the suggested IO-linearization also achieves full state linearization.

## Chapter 4

# Controller design

### 4.1 Control strategy

In chapter 3 it appears that the H-drive can be controlled by means of IO-linearization. According to [1] this is practically not the case because the controller is not able to suppress all unmodelled influences such as friction and cogging. Therefore in [1] the so-called "virtual internal model following control" approach according to [3] is adopted. In Figure 4.1 the control structure of this approach is shown. In this structure the result

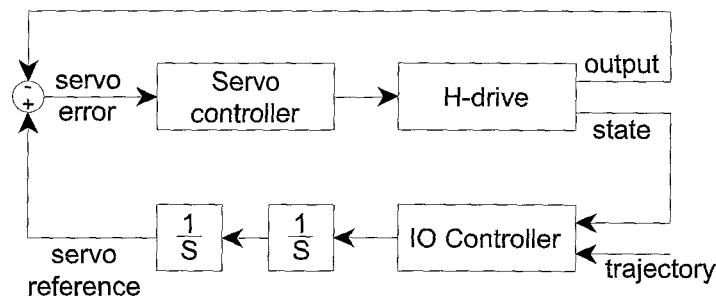


Figure 4.1: Control structure of the H-drive. source [4]

of the high level IO-controller (desired acceleration) is integrated twice to generate a reference trajectory for the low level servo controller. For the H-drive the low level servo controller, derived in [6], consists of three feed forward controllers of the type PI lead/lag in series with a second-order low-pass with a cutt-off frequency at 300 Hz and are given by:

$$C_{servo,X} = \frac{0.6755s^2 + 106.1s + 4000}{4.4806 \cdot 10^{-9}s^3 + 1.6892 \cdot 10^{-5}s^2 + 1.5920 \cdot 10^{-2}s} \quad (4.1)$$

$$C_{servo,Y} = \frac{1.182s^2 + 185.7s + 7000}{4.4806 \cdot 10^{-9}s^3 + 1.6892 \cdot 10^{-5}s^2 + 1.5920 \cdot 10^{-2}s}$$

Note that the controller of the X-LiMMS is only in gain different from the two identical Y-LiMMS controllers because the mass in the Y-axes is larger than in the X-axis.

## 4.2 IO controller

The exact construction of the IO controller, mentioned in section 4.1, is depicted in figure 4.2. The IO linearizing control law  $\underline{u}$  is already computed in chapter 3. To

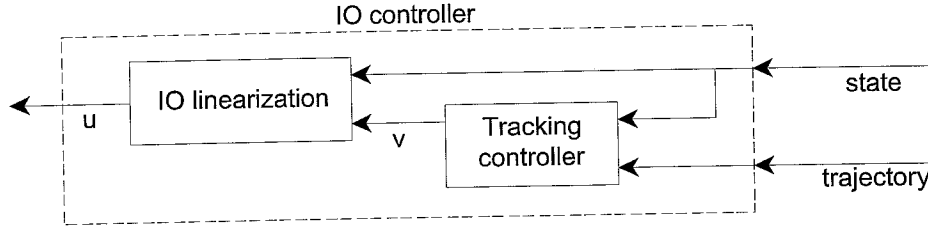


Figure 4.2: H-drive IO Controller structure. source [4]

complete the IO controller an appropriate tracking controller has to be obtained.

As seen in (3.9) the state feedback control law  $\underline{u}$  converts the system into the (closed loop) decoupled system

$$\begin{bmatrix} \ddot{y}_1 \\ \ddot{y}_2 \\ \ddot{y}_3 \end{bmatrix} = \begin{bmatrix} v_1 \\ v_2 \\ v_3 \end{bmatrix}. \quad (4.2)$$

This means that the result of the IO controller represents a corrective acceleration such that, for an appropriate  $\underline{v}$ , the real trajectory converges to the desired trajectory. The first and the third component of (4.2) represent the corrective acceleration of the X-LiMMS in respectively the  $\bar{e}_1$  and  $\bar{e}_2$  direction, see figure 2.1. The second component of (4.2) represents the corrective angular acceleration of the beam.

If the X-LiMMS has to perform a desired trajectory described by  $[Y_d(t), X_d(t)] \bar{e}$  then the IO controller has to provide a set of corrective accelerations such that the real trajectory  $[Y(t), X(t)] \bar{e}$  converges to this desired trajectory. To do this the tracking controllers

$$v_1 = \ddot{Y}_d(t) - a_2 \dot{e}_Y(t) - a_1 e_Y(t) \quad , \quad v_3 = \ddot{X}_d(t) - a_4 \dot{e}_X(t) - a_3 e_X(t) \quad (4.3)$$

can be used. In these equations  $e_Y(t)$  and  $e_X(t)$  represent the tracking errors defined by  $e_Y(t) = Y(t) - Y_d(t)$  and  $e_X(t) = X(t) - X_d(t)$ . The coefficients  $a_1, a_2, a_3$  and  $a_4$  have to be chosen so that the polynomials

$$\lambda^2 + a_2 \lambda + a_1 \quad , \quad \lambda^2 + a_4 \lambda + a_3 \quad (4.4)$$

are Hurwitz i.e. the polynomials have all roots in the open left-half plane.

For the second term in (4.2), the angular acceleration, a different controller has to be defined.

$$v_2 = -a_6\dot{\varphi} - a_5e_\varphi(t) \quad (4.5)$$

The purpose of this controller is to stabilize the angle of the beam at  $\varphi_d$ . In the equation represents  $e_\varphi(t)$  the tracking error  $\varphi(t) - \varphi_d$ . The coefficients  $a_5$  and  $a_6$  have to be chosen so that  $\lambda^2 + a_6\lambda + a_5$  is Hurwitz. Note that in the most situations  $\varphi_d = 0$ .

Summarizing the preceding results the tracking controller for the IO-linearization can be defined as

$$\begin{bmatrix} v_1 \\ v_2 \\ v_3 \end{bmatrix} = \begin{bmatrix} \ddot{Y}_d \\ 0 \\ \ddot{X}_d \end{bmatrix} - k_2 \begin{bmatrix} \dot{e}_Y \\ \dot{\varphi} \\ \dot{e}_X \end{bmatrix} - k_1 \begin{bmatrix} e_Y \\ e_\varphi \\ e_X \end{bmatrix} \quad (4.6)$$

where

$$k_2 = \begin{bmatrix} a_2 & 0 & 0 \\ 0 & a_6 & 0 \\ 0 & 0 & a_4 \end{bmatrix}, \quad k_1 = \begin{bmatrix} a_1 & 0 & 0 \\ 0 & a_5 & 0 \\ 0 & 0 & a_3 \end{bmatrix} \quad (4.7)$$

In theory the poles (roots) can be placed anywhere in the left-half plane but in practice this is not the case. The limitation of the pole position will be determined by the sampling frequency of the system. A higher sampling frequency makes a pole placement further in the left-half plane possible.



## Chapter 5

# Simulations and Experiments

To test the controller strategy, sketched in figure 4.1, a Simulink program is made (Appendix E). This program contains the controller, a reference trajectory generator and a H-drive block which is either a link to the physical H-drive or the H-drive model from chapter 2.

The first thing that will be discussed in this chapter is the reference trajectory that was used for the simulation and experiment. Secondly, the used construction parameters are summarized. In the last two sections the simulation and the experimental results will be presented.

### 5.1 Reference trajectory

Before a computer simulation or experiment can be done one has to choose an appropriate reference trajectory. The reference trajectory has to offer the possibility to test the stabilization and tracking capability of the controller. For simplicity a circular trajectory of the X-LiMMS as in figure 5.1 is chosen. The reference tilt angle is kept equal to zero (no tilt of the beam).

To indicate different stages in the trajectory description the numbers 1,2 and 3 are added to figure 5.1. The stabilization property can be evaluated from the origin (point 1) to the starting point of the circle trajectory, point 3. As can be seen in figure 5.1 the X-LiMMS reference position stays the same from point 2 to 3, so the controller has the opportunity to stabilize at this position. The tracking property can be evaluated during the circular motion which is started at point 3.

In figure 5.2 the reference trajectory of the X-LiMMS in the x- and y-direction is depicted. The points 1, 2 and 3 represent the same positions as the ones in figure 5.1. In figure 5.2 the points 4 and 5 are added to indicate significant points for the circle trajectory. In the first part of the trajectory, point 1-2, the X-LiMMS is moved tot a starting

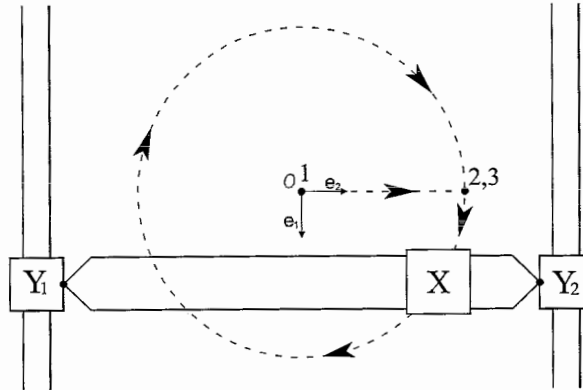


Figure 5.1: Reference trajectory for the computer simulation and experiment

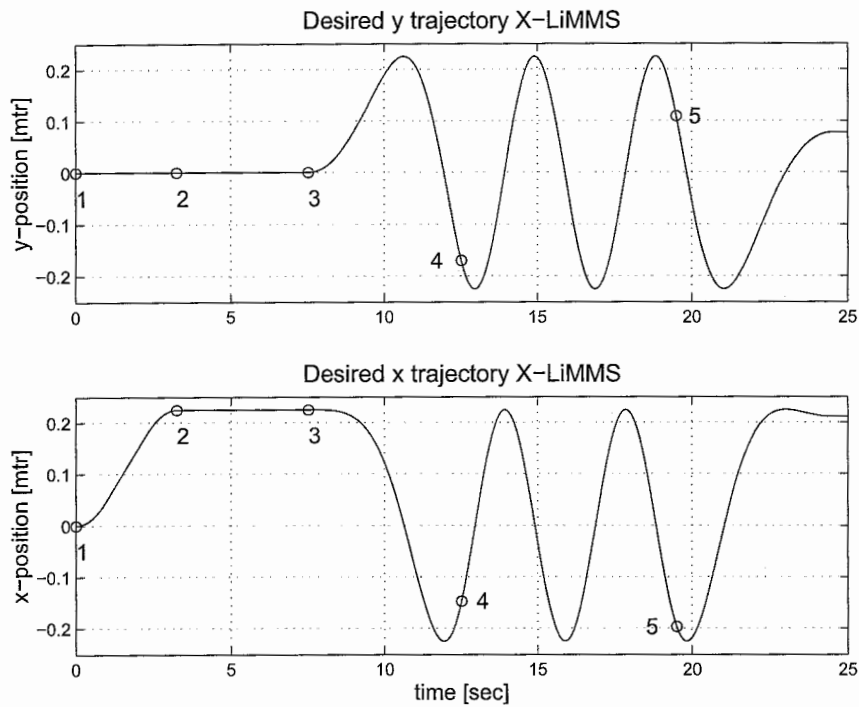


Figure 5.2: Reference trajectories for the x- and y-position of the X-LiMMS

position on the circle trajectory. The second part, point 2-3, allows the controller to stabilize the X-LiMMS at the starting position. At point 3 the X-LiMMS starts accelerating ( $a = 0.32[\text{rad}/\text{sec}^2]$ ) on the circular trajectory. At point 4 the X-LiMMS is rotating with a frequency of  $0.25[\text{Hz}]$ . This rotational speed is maintained until point 5 is reached where the deceleration starts until the speed of the X-LiMMS equals zero.

## 5.2 Parameters

To make the controller operational values for the construction parameters have to be chosen. Table 5.2 is a summary of the used values. These values are determined in [1] using a linear least-squares identification procedure.

parameter	value
$D$	0.3 [m]
$m_{y1}$	9.12 [kg]
$m_{y2}$	9.12 [kg]
$m_x$	9.12 [kg]
$m_b$	32.08 [kg]
$J_b$	0.9624 [kg · m <sup>2</sup> ]
$k_m$	74.4 [N/A]

Table 5.1: Parameter values used for the simulation and experiment

A tool that can be used to tune the behavior of the H-drive is the placement of the tracking controller poles. The pole positions that are used for the simulation and experiment are the same. For the  $y$  and  $x$  tracking controller both poles are placed at  $-85$ . For the tracking controller of the beam angle  $\varphi$  both poles were placed at  $-80$ . The coefficient matrices of equation (4.7) result, with the proposed placement of the poles, in:

$$k_2 = \begin{bmatrix} 170 & 0 & 0 \\ 0 & 160 & 0 \\ 0 & 0 & 170 \end{bmatrix}, \quad k_1 = \begin{bmatrix} 7225 & 0 & 0 \\ 0 & 6400 & 0 \\ 0 & 0 & 7225 \end{bmatrix} \quad (5.1)$$

## 5.3 Simulation results

Prior to the experiment a simulation is done to check the functionality of the controller and to generate data that can be compared to the results of the experiment. By comparing the results of the simulation and experiment a conclusion can be made with respect to the correctness of the in chapter 2 derived H-drive model.

In figure 5.3 the tracking error of the simulation is shown. It can be seen that the tracking error during the acceleration of the X-LiMMS in the x-direction (figure 5.3:  $x - x_{ref}$ , stabilization part) stabilizes towards a nonzero value. This phenomenon is probably caused by the feedforward of the tracking controller and the PID-controller. At the constant speed and hold position parts, the tracking error converges quickly towards zero. The figure shows also that the maximum error occurs at the highest speed.

Figure 5.4 shows the total state feedback  $u$  and the feedforward part of the state feedback which is utilized in the tracking controller (equation (4.3): desired acceleration).

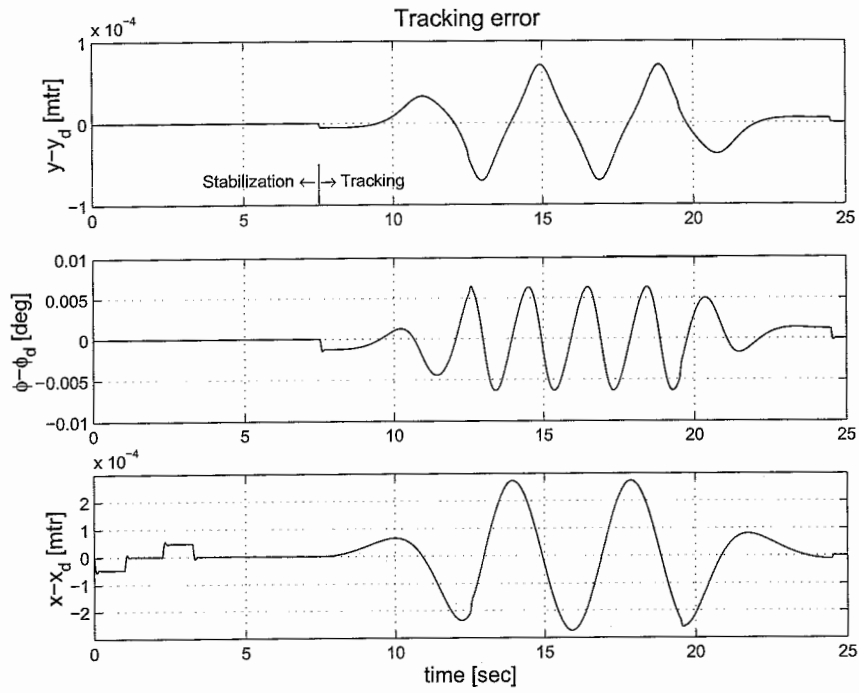


Figure 5.3: Simulation: Tracking error

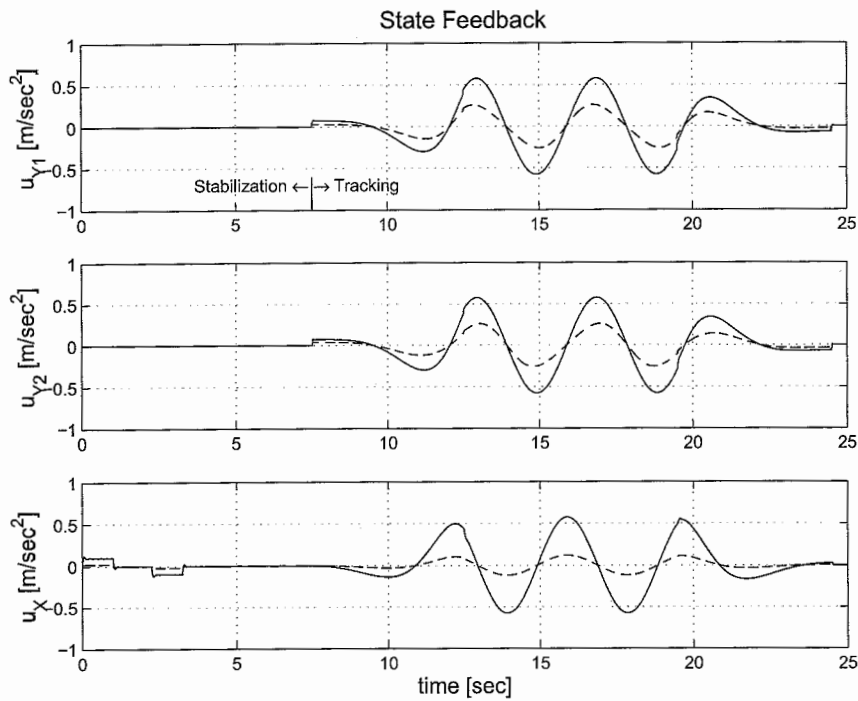


Figure 5.4: Simulation: Total state feedback  $u$  (continuous) and the feedforward part of the state feedback (dashed)

Observe that the feedforward for the angle of the beam equals zero.

In figure 5.5 the currents to the LiMMS are shown. The "disturbances" in the plot

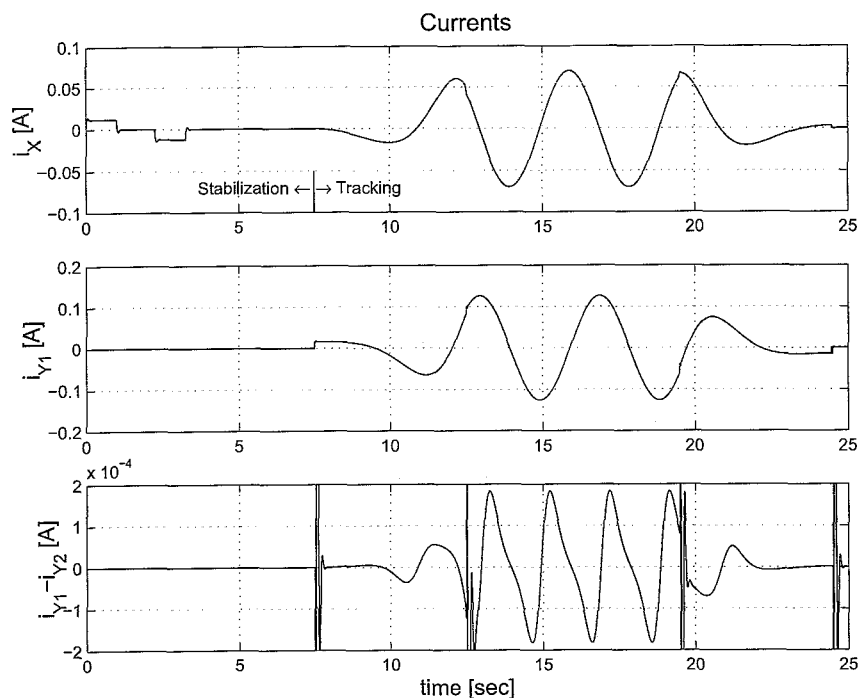


Figure 5.5: Simulation: Currents  $i_x$ ,  $i_{y1}$  and  $i_{y1} - i_{y2}$

for  $i_{y1} - i_{y2}$  are reflections of the step response of the PID-controller caused by the suddenly changing accelerations of the LiMMS. It can also be noticed that the difference between the currents  $i_{y1}$  and  $i_{y2}$  are relatively small in relation to the current  $i_{y1}$ .

## 5.4 Experimental results

To prove the reliability of the designed controller an experiment is done with the H-drive in the Dynamics and Control Technology laboratory of the departement Mechanical Engineering. The parameters and pole placements that where used for this experiment are exactly the same as the ones used for the simulation.

In this section the experimental results are presented. Figure 5.6 shows the tracking error. At the start of the time axis the tracking error contains a peak value. This is the correction that the controller makes on the initial position. During the acceleration and deceleration of the X-LiMMS one can observe that the tracking error converges towards a steady level. This phenomenon is also observable in the simulation results and is caused by the tracking and the PID-controller.

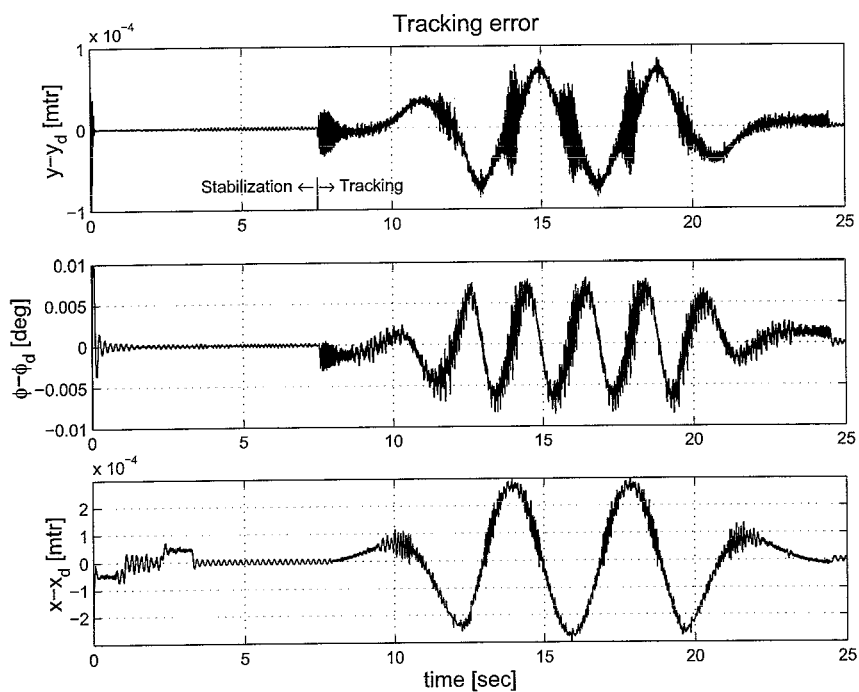


Figure 5.6: Experiment: Tracking error

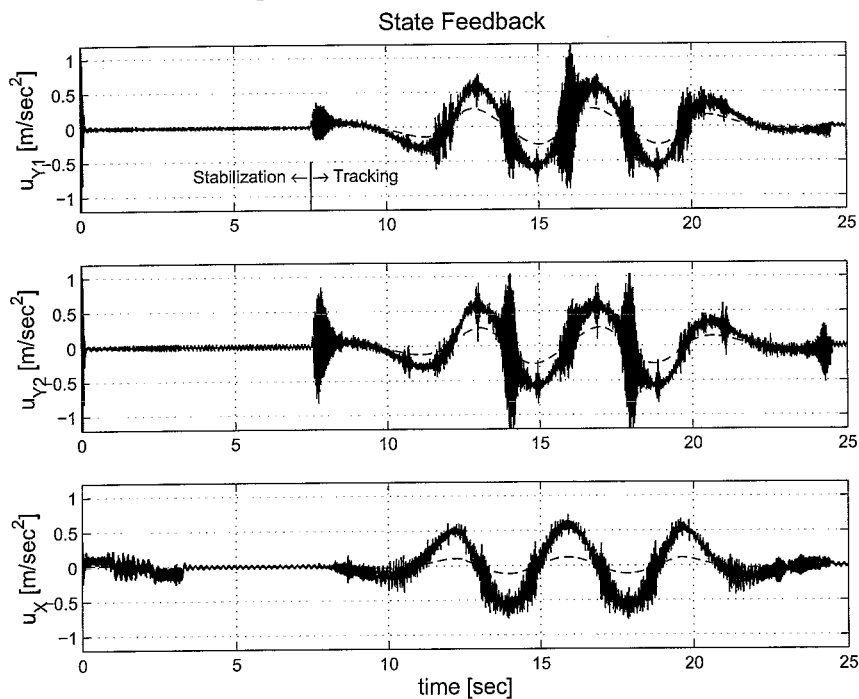


Figure 5.7: Experiment: Total state feedback  $u$  (continuous) and the feedforward part of the state feedback (dashed)

In the timespan (3.25-7.5 [sec]) in which the controller can stabilize the X-LiMMS the tracking error forms a sinusoidal signal. The amplitude of this sinusoidal signal is probably the limit of the controller accuracy. The amplitude of this sinusoidal signal is influenced by the pole position. When the poles are placed far in the left-half plane then the gain  $k_1$  of the position error is large which mean that the control action  $v_3$  for small position error is also relatively large. The consequence of this is that the X-LiMMS starts oscillating around the desired position.

At the time where the X-LiMMS is starting to perform the circle trajectory (time 7.5 [sec]) the tracking errors in the  $y$  and  $\varphi$  direction show a disturbance which is caused by the acceleration of the  $y$  axis. Because the X-LiMMS is positioned out of the center, the controller needs to send out different currents to the Y1 and Y2-LiMMS. The disturbance is caused by the convergence proces to these different currents.

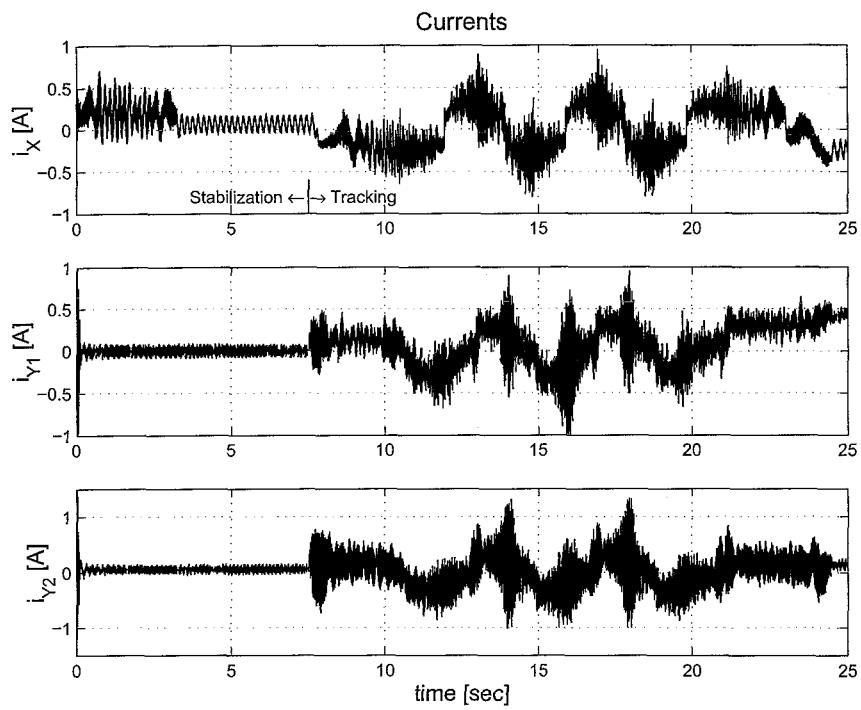
Remarkable are the three disturbances in the  $y - y_{ref}$  plot that occur at the times 14, 16 and 18 seconds. At these times  $x - x_{ref}$  reaches a maximum caused by the change of direction of the X-LiMMS. During this change of direction the acceleration of the X-LiMMS reaches a maximum.

The main conclusion regarding the tracking error is that the tracking error of the  $y$ - and  $x$ -axis is strongly related to the imposed acceleration. The angular tracking error  $\varphi - \varphi_{ref}$  is caused and thus related to the position of the X-LiMMS.

In the state feedback  $u$ , figure 5.7, the mutually dependence is even more present. The main difference of this plot with the one of the tracking error plot is the come-back of the peaks, at times 14, 16 and 18 seconds, in the  $u_{Y2}$ -plot. Moreover it can be concluded that amplification of the feedforward, the dashed line in the  $v_1$  and  $v_3$  plot will leads to a smaller tracking error and less noise in the current plot, figure 5.8. This conclusion can be made because the tracking error shows a strong relationship to the imposed accelerations (feedforward). To investigate the previous conclusion the experiment is repeated for a larger feedforward. The results are shown in appendix D.

The current plot is not providing as much insight as the previous plots but a few remarks can be made. During the stabilization the  $i_X$  current oscillates between an upper and lower level with a frequency of approximately  $0.45[Hz]$ . The mean current is approximately  $0.06[Amp]$ . The exact source of this oscillation is hard to determine but a relation to friction and/or cogging is not excluded. When comparing the  $i_{Y1}$  and  $i_{Y2}$  currents one can notice that the global amplitude of the  $i_{Y2}$  current is larger. This can mean that the Y2-LiMMS is subject to larger friction or cogging forces or simply has a bigger mass.

At the end of the experiment, when the LiMMS come to rest, a strange phenomena occurs. The current starts floating away form zero while the position is maintained. The controller has possibly converged to a frequency which allows the current to float away while the position is held.

Figure 5.8: Experiment: Currents  $i_x$ ,  $i_{y1}$  and  $i_{y2}$



## Chapter 6

# Conclusions and Recommendations

### 6.1 Conclusions

The experiment has shown that the suggested control strategy can be employed on the H-drive. The experimental results are, what tracking error concerns, satisfying but some tuning of the used parameters, pole placements and the amplification of the feedforwards (appendix D) can improve the experimental results. The drift of the  $i_{Y1}$  and  $i_{Y2}$  current is stil an unsolved problem which possibly can be suppressed with a low pass frequency filter between the controller output and the H-drive input.

When comparing the results of the simulation and experiment it appears that the similarity is strong. It is obvious that the experimental results are more noisy, but this seems logical. The similarity of the current plots is not very good. The current applied on the LiMMS during the experiment is significantly lager than the current in the simulation. This is probably caused by the friction and cogging forces which the H-drive is subject to.

To give an impression of the accuracy of the developed controller a comparison with experimental results of another controller type can be made. When doing this attention should be paid to the level of development and additional features of this reference controller. In [2] Iterative Learning Control (ILC) is applied on the H-drive. The basic controller used in [2] consist of a PID type controller with a low pass filter and two notches. Parallel to this basic controller a ILC controller is installed. To determine the effect of the ILC several experiments in [2] are done. The results of the first experiment in which no ILC is applied can be used as a reference for the in this report developed controller. In this experiment a third order point to point trajectory for the X-LiMMS is defined. The maximum jerk, acceleration, velocity and displacement are respectively  $100[m/s^3]$ ,  $7.1[m/s^2]$ ,  $0.5[m/s]$  and  $0.29[m]$ . The maximal displacement error on the

desired third order trajectory is of order  $1 \cdot 10^{-4}[m]$ . The average displacement error is approximately  $5 \cdot 10^{-5}[m]$ . This means that the order of the displacement error of this experiment is roughly the same as the one of the experimental results obtained with the feedforward gain. However the trajectory performed in [2] imposes larger accelerations and speeds than the one performed in this report. The performance of the controller used in [2] will therefore perform better than the one developed in this report. This can change when the model parameters and feedforward are better tuned.

## 6.2 Recommendations

During the development of the H-drive model and controller several issues that can lead to improvement of the experiment are noticed. A correction, regarding the H-drive model, that could improve the correspondence of the model and the H-drive is the modelling of the total rotational inertia. In this thesis the center of total rotational inertia is placed in the middle of the beam. The hinge of the Y1- or Y2-LiMMS will be a better position because the beam rotates mostly around these hinges.

When studying the experimental results it appears that the determination of the rotational speed produces noisy results. It is not clear if the produced signal is correct or that the differentiation causes errors. Attempts to improve the results by inserting a low pass filter did only aggravate the problem. Investigation of the correctness of the rotational speed determination can improve the experiment because the noise in the state variable only will be amplified in the input-output controller which deteriorates the feedback linearization.

## Appendix A

# Results of the Lagrange equations of motion

In chapter 2 the Lagrange equations of motion are derived. In this appendix some results are presented.

### A.1 Kinetic energy

The kinetic energy for the H-drive, as derived in equation 2.4, can be written out as

$$\begin{aligned} T = & \frac{1}{2}m_b\dot{y}^2 + \frac{1}{2}m_{y1}(\dot{y} + D(1 + \tan^2(\varphi))\dot{\varphi})^2 + \frac{1}{2}m_{y2}(\dot{y} - D(1 + \tan^2(\varphi))\dot{\varphi})^2 \\ & + \frac{1}{2}m_x((\dot{y} + (D(1 + \tan^2(\varphi)) - x \cos(\varphi))\dot{\varphi} - \sin(\varphi)\dot{x})^2 + \\ & (-x \sin(\varphi)\dot{\varphi} + \cos(\varphi)\dot{x})^2) + \frac{1}{2} \left( J_b + m_x \left( x - \left( \frac{D}{\cos(\varphi)} \right)^2 \right) \right) \dot{\varphi}^2. \end{aligned} \quad (\text{A.1})$$

### A.2 Lagrange equations of motion

In (2.8) the Lagrange equations of motion are rewritten in matrix/vector form. In this equation  $\underline{M}(\underline{q})$  represents the mass-matrix.  $\underline{C}(\underline{q}, \underline{\dot{q}})$  contains the coriolis and centripetal terms and  $\underline{g}(\underline{q})$  encompasses joint flexibility and gravitational effects. The vector  $\underline{\tau}$  represents the applied forces and torques, derived from  $\underline{Q}^{nc}$ . If  $\underline{C}(\underline{q}, \underline{\dot{q}})$  and  $\underline{g}(\underline{q})$  are combined in one term  $\underline{H}(\underline{q}, \underline{\dot{q}})$  and  $\underline{\tau}$  is split up in  $\underline{Bu}$  the matrices  $\underline{M}$ ,  $\underline{B}$  and the vector

$H$  will be given by:

$$\begin{aligned}
M_{[11]} &= m_b + m_x + m_{y1} + m_{y2} \\
M_{[12]} &= \frac{-1}{\cos^2(\varphi)} (D(m_{y2} - m_{y1} - m_x)) - m_x x \cos(\varphi) \\
M_{[13]} &= -m_x \sin(\varphi) \\
M_{[21]} &= \frac{-1}{\cos^2(\varphi)} (D(m_{y2} - m_{y1} - m_x)) - m_x x \cos(\varphi) \\
M_{[22]} &= 2m_x x^2 - \frac{4}{\cos(\varphi)} m_x x D + \frac{1}{\cos^4(\varphi)} (D^2(m_{y1} + m_{y2} + (1 + \cos^2(\varphi))m_x) + J_b) \\
M_{[23]} &= \frac{-m_x D \sin(\varphi)}{\cos^2(\varphi)} \\
M_{[31]} &= -m_x \sin(\varphi) \\
M_{[32]} &= \frac{-m_x D \sin(\varphi)}{\cos^2(\varphi)} \\
M_{[33]} &= m_x
\end{aligned} \tag{A.2}$$

$$B = k_m \begin{bmatrix} 1 & 1 & -\sin(\varphi) \\ D(1 + \tan(\varphi))^2 & -D(1 + \tan(\varphi))^2 & -D \sin(\varphi) / \cos^2(\varphi) \\ 0 & 0 & 1 \end{bmatrix} \tag{A.3}$$

$$\begin{aligned}
H_{[1]} &= \frac{\dot{\varphi}}{\cos^3(\varphi)} (-2m_x \cos^4(\varphi) \dot{x} + (2D(m_x + m_{y1} - m_{y2}) + \cos^3(\varphi) m_x x) \dot{\varphi} \sin(\varphi)) \\
H_{[2]} &= \frac{-\dot{\varphi}}{\cos^5(\varphi)} ((4m_x \cos^4(\varphi) \dot{x} + (2(-m_x - m_{y1} - m_{y2}) - m_x \cos^2(\varphi)) \sin(\varphi) \dot{\varphi} D) D + \\
&\quad (-4 \cos^5(\varphi) m_x \dot{x} + 2m_x D \sin(\varphi) \dot{\varphi} \cos^3(\varphi) x) \\
H_{[3]} &= \frac{-m_x \dot{\varphi}^2}{\cos^3(\varphi)} ((-3 \cos^2(\varphi) + 2) + 2 \cos^3(\varphi) x)
\end{aligned} \tag{A.4}$$

## Appendix B

# Results of the IO linearization

### B.1 The matrix $A(x)$ and vector $N(x)$

Using (3.6) the matrix  $A(x)$  and the vector  $N(x)$  for the H-drive will be given:

$$\begin{aligned}
A_{[11]} &= \cos^2(\varphi)k_m(\cos^4(\varphi)J_b + (m_b + 4m_{y2} + m_x \cos^2(\varphi))D^2 + \\
&\quad ((-\cos(\varphi)m_b - 2m_x \cos^3(\varphi) - 2\cos(\varphi)m_{y2})D + \cos^4(\varphi)m_x x)/\alpha \\
A_{[12]} &= \cos^2(\varphi)k_m(\cos^4(\varphi)J_b + (m_x \cos^2(\varphi) - m_b)D^2 + \\
&\quad ((-2m_x \cos^3(\varphi) + 2\cos(\varphi)m_{y1} + \cos(\varphi)m_b)D + \cos^4(\varphi)m_x x)/\alpha \\
A_{[13]} &= -\sin(\varphi)k_m/m_x \\
A_{[21]} &= k_m \cos^2(\varphi)((m_b + 2m_{y2})D + m_x x \cos^3(\varphi)/\alpha \\
A_{[22]} &= k_m \cos^2(\varphi)((-2m_{y1} - m_b - 2m_x \cos^2(\varphi))D + m_x x \cos^3(\varphi)/\alpha \\
A_{[23]} &= 0 \\
A_{[31]} &= \sin(\varphi)k_m \cos(\varphi)(\cos^4(\varphi)J_b + (m_b + 4m_{y2} + m_x \cos^2(\varphi))D^2 \\
&\quad + ((-\cos(\varphi)m_b - 2m_x \cos^3(\varphi) - 2\cos(\varphi)m_{y2})D + \cos^4(\varphi)m_x x)/\alpha \\
A_{[32]} &= \sin(\varphi)k_m \cos(\varphi)(\cos^4(\varphi)J_b + (m_x \cos^2(\varphi) - m_b)D^2 + \\
&\quad ((-2m_x \cos^3(\varphi) + 2\cos(\varphi)m_{y1} + \cos(\varphi)m_b)D + \cos^4(\varphi)m_x x)/\alpha \\
A_{[33]} &= \cos(\varphi)k_m/m_x
\end{aligned} \tag{B.1}$$

where

$$\begin{aligned}
\alpha &= ((m_{y2} + m_{y1} + m_b) \cos^4(\varphi) + \cos^6(\varphi)m_x)J_b \\
&\quad + (m_b m_{y2} + (4m_{y2} + m_b)m_{y1} + ((5m_{y2} + m_{y1} + 2m_b) \cos^2(\varphi) + \cos^4(\varphi)m_x)m_x D^2 \\
&\quad + (((-6m_{y2} - 2m_{y1} - 4m_b) \cos^3(\varphi) - 2\cos^5(\varphi)m_x)m_x D \\
&\quad + (2(m_{y2} + m_{y1} + m_b) \cos^4(\varphi) + \cos^6(\varphi)m_x)m_x x)
\end{aligned} \tag{B.2}$$

$$\begin{aligned}
N_{[1]} &= -\dot{\varphi}(2(m_b J_b + m_{y2} J_b + m_{y1} J_b) \cos^6(\varphi) \dot{x} + \\
&\quad ((-5m_{y2} J_b - 3m_b J_b - m_{y1} J_b) \cos^4(\varphi) \sin(\varphi) \dot{h} + ((2m_b m_{y2} + (2m_b + 8m_{y2})m_{y1} + \\
&\quad 2(m_{y1} - m_{y2})m_x \cos^2(\varphi)) \cos^2(\varphi) \dot{x} + (m_b m_{y2} + (-4m_{y2} - m_b)m_{y1} + \\
&\quad (m_{y1} - 3m_{y2} - 2m_b)m_x \cos^2(\varphi)) \sin^2(\varphi) \dot{\varphi} D) D) D + \\
&\quad ((m_{y1} J_b + m_b J_b + m_{y2} J_b) \cos^5(\varphi) \sin(\varphi) \dot{\varphi} + (2(-m_{y1} + m_{y2})m_x \cos^5(\varphi) \dot{x} + \\
&\quad (-m_b m_{y2} + (-4m_{y2} - m_b)m_{y1} + \\
&\quad (10m_{y2} + 2m_{y1} + 6m_b)m_x \cos^2(\varphi)) \cos(\varphi) \sin(\varphi) \dot{\varphi} D) D + \\
&\quad ((-9m_{y2} - 6m_b - 3m_{y1})m_x \cos^4(\varphi) \sin(\varphi) \dot{\varphi} D + \\
&\quad (2m_{y2} + 2m_{y1} + 2m_b)m_x \cos^5(\varphi) \sin(\varphi) \dot{\varphi} x) x) / \beta \\
N_{[2]} &= \dot{\varphi}(((4m_b + 2m_{y1} + 6m_{y2})m_x + 2m_x^2 \cos^2(\varphi)) \cos^4(\varphi) \dot{x} + \\
&\quad (-2m_b m_{y2} + (-2m_b - 8m_{y2})m_{y1} + \\
&\quad ((-11m_{y2} - m_{y1} - 4m_b)m_x - m_x^2 \cos^2(\varphi)) \cos^2(\varphi) \sin(\varphi) \dot{\varphi} D) D + \\
&\quad ((4(-m_{y1} - m_{y2} - m_b)m_x - 2m_x^2 \cos^2(\varphi)) \cos^5(\varphi) \dot{x} + \\
&\quad (4m_b + m_{y1} + 7m_{y2})m_x \cos^2(\varphi) \sin(\varphi) \dot{\varphi} D + m_x^2 \cos^6(\varphi) \dot{\varphi} \sin(\varphi) x) x) / \beta \\
N_{[3]} &= \dot{\varphi}((-2m_b - 2m_{y2} - 2m_{y1}) J_b \cos^5(\varphi) \sin(\varphi) \dot{x} + \\
&\quad (J_b(2m_b + 4m_{y2} + (-m_x - 5m_{y2} - 3m_b - m_{y1}) \cos^2(\varphi)) \cos^3(\varphi) \dot{\varphi} + \\
&\quad ((-2m_b m_{y2} + (-2m_b - 8m_{y2})m_{y1} + (-2m_{y1} + 2m_{y2})m_x \cos^2(\varphi)) \cos(\varphi) \sin(\varphi) \dot{x} + \\
&\quad (-m_b m_{y2} + (-4m_{y2} - m_b)m_{y1} - 2m_x m_{y2} + \\
&\quad (-m_{y1} - 3m_{y2} - 2m_b - m_x)m_x \cos^2(\varphi)) \cos(\varphi) \dot{\varphi} D) D) D + \\
&\quad ((m_x + m_{y1} + m_b + m_{y2}) J_b \cos^6(\varphi) \dot{\varphi} + (2(m_{y1} - m_{y2})m_x \cos^4(\varphi) \sin(\varphi) \dot{x} + \\
&\quad (2m_b m_{y2} + (2m_b + 8m_{y2})m_{y1} + (-m_b m_{y2} + (-4m_{y2} - m_b)m_{y1} + (m_{y2} + m_{y1})m_x + \\
&\quad (10m_{y2} + 2m_{y1} + 6m_b + 3m_x)m_x \cos^2(\varphi)) \cos^2(\varphi) \dot{\varphi} D) D + \\
&\quad (((m_{y2} - m_{y1})m_x + (-9m_{y2} - 6m_b - 3m_{y1} - 3m_x)m_x \cos^2(\varphi)) \cos^3(\varphi) \dot{\varphi} D + \\
&\quad (2m_{y2} + 2m_{y1} + 2m_b + m_x)m_x \cos^6(\varphi) \dot{\varphi} x) x) / \beta \tag{B.3}
\end{aligned}$$

where

$$\begin{aligned}
\beta &= \cos(\varphi)((m_{y1} + m_{y2} + m_b + m_x \cos^2(\varphi)) J_b \cos^4(\varphi) + \\
&\quad (4m_{y1} m_{y2} + ((5m_{y2} + m_{y1})m_x + m_x^2 \cos^2(\varphi)) \cos^2(\varphi) + \\
&\quad (m_{y1} + m_{y2} + 2m_x \cos^2(\varphi)) m_b) D^2 + \\
&\quad (((-6m_{y2} - 2m_{y1})m_x - 2m_x^2 \cos^2(\varphi)) \cos^3(\varphi) - 4m_b \cos^3(\varphi) m_x) D + \\
&\quad ((2(m_{y2} + m_{y1})m_x + m_x^2 \cos^2(\varphi)) \cos^4(\varphi) + 2m_b \cos^4(\varphi) m_x) x) \tag{B.4}
\end{aligned}$$

## B.2 Non-singularity proof $A(x)$

The matrix  $A(x)$  has to be non-singular in the working area because an inverse must exist. Non-singularity of this matrix can be investigated with its determinant because the determinant of a singular matrix equals zero. The determinant of  $A(x)$  is given by

$$\begin{aligned}
 \det(A) &= \text{numerator}/\text{denominator} \\
 \text{numerator} &= -2Dk_m^3 \cos^3(\varphi) \\
 \text{denominator} &= \cos^6(\varphi)(m_x^2(J_b + x^2)) - \cos^5(\varphi)2Dm_x^2x \\
 &\quad + \cos^4(\varphi)((m_{y1} + m_{y2} + m_b)((m_x + 1)m_x x^2 + m_x J_b) + m_x^2 D^2) \\
 &\quad - \cos^3(\varphi)2Dm_x(m_{y1} + m_{y2} + m_b + m_x(m_b + 2m_{y2})) \\
 &\quad + \cos^2(\varphi)D^2 m_x(m_{y1} + m_{y2} + m_b + m_x(m_b + 4m_{y2})) \\
 &\quad + m_x D^2(4m_{y1}m_{y2} + m_b(m_{y1} + m_{y2})). \tag{B.5}
 \end{aligned}$$

Its easy to see that for  $\varphi = \pm\frac{\pi}{2}$  the numerator of the determinant equals zero, i.e.  $A(x)$  is singular. Note that this angle of the beam physically impossible is.

When observing (B.5) the conclusion can be made that the ratio of the numerator and denominator is also important because a sharp raise of the denominator can cause near singularity of  $A(x)$ . To investigate the previous observation a few constants are introduced.

$$\begin{aligned}
 c_1 &= -2Dk_m^3 \\
 c_2 &= m_x^2 J_b \\
 c_3 &= -2Dm_x^2 \\
 c_4 &= (m_{y1} + m_{y2} + m_b)(m_x + 1)m_x \\
 c_5 &= (m_{y1} + m_{y2} + m_b)m_x J_b + D^2 m_x^2 \\
 c_6 &= -2Dm_x(m_{y1} + m_{y2} + m_b + m_x(m_b + 2m_{y2})) \\
 c_7 &= D^2 m_x(m_{y1} + m_{y2} + m_b + m_x(m_b + 4m_{y2})) \\
 c_8 &= D^2 m_x(4m_{y1}m_{y2} + m_b(m_{y1} + m_{y2})) \tag{B.6}
 \end{aligned}$$

Using these constants and the coordinate transformation  $[z, x]^T = [\cos(\varphi), x]$  the determinant of  $A(x)$  can be written like

$$\det(A) = \frac{c_1 z^3}{(m_x^2 x^2 + c_2)z^6 + c_3 x z^5 + (c_4 x^2 + c_5)z^4 + c_6 x z^3 + c_7 z^2 + c_8}. \tag{B.7}$$

Calculation of the constants, using the H-drive parameters in table B.1, and numerical analysis of the determinant for a range of work area coordinates shows that determinant is only small around the singularity point  $\varphi = \pm\frac{1}{2}\pi$ . In figure B.1 the numerical results for a space spanned by  $x = [0.05, 0.55]$  and  $\varphi = [-\frac{1}{2}\pi, \frac{1}{2}\pi]$  are shown.

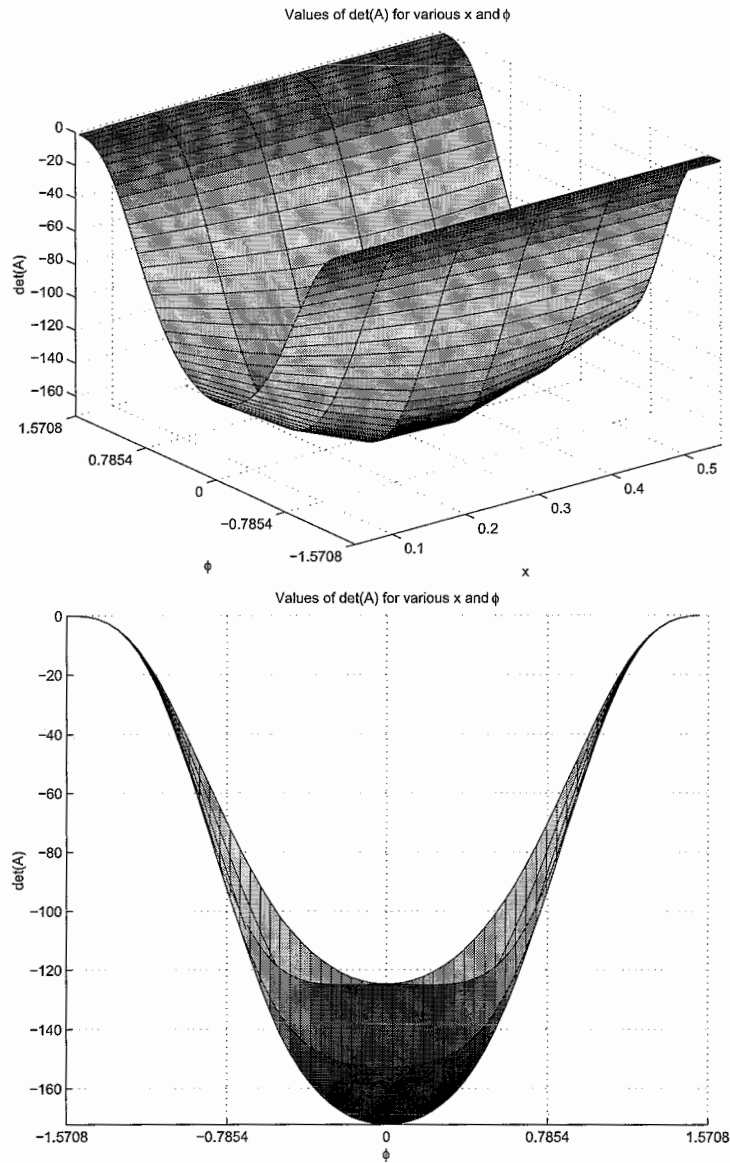


Figure B.1: Determinant value of  $A(x)$  for a workspace spanned by  $\varphi = [-\frac{1}{2}\pi, \frac{1}{2}\pi]$ ,  $x = [0.05, 0.55]$ , above: 3d view of  $det(A)$ ,  $\varphi$  and  $x$ , below: 2d view of  $det(A)$  and  $\varphi$



parameter	value
$k_m$	74.4 [N/A]
$m_{y1}$	9.12 [kg]
$m_{y2}$	9.12 [kg]
$m_x$	9.12 [kg]
$m_b$	32.08 [kg]
$J_b$	0.9624 [kgm <sup>2</sup> ]
$D$	0.3 [m]

Table B.1: H-drive system parameters used for the numerical non-singularity analysis

### B.3 The state feedback law

As seen in chapter 3 the state feedback control law of the H-drive can be written as

$$u = A^{-1}(x)[v - N(x)] \quad (\text{B.8})$$

The state feedback control law  $\underline{u}$  for the H-drive according (B.8) will be given

$$\begin{aligned}
u_{[1]} &= \frac{1}{2Dk_m \cos^2(\varphi)} (-D^2 m_b (v_2 \cos(\varphi) + 2 \sin(\varphi) \dot{\varphi}^2) - m_x \cos^6(\varphi) x v_1 \\
&\quad + \cos^2(\varphi) (\dot{x} \dot{\varphi} D (4m_{y1} + 2m_b) + D x v_2 (2m_{y1} + m_b) + \\
&\quad D \sin(\varphi) v_3 (m_b + 2m_{y1}) + 3D^2 \dot{\varphi}^2 \sin(\varphi)) \\
&\quad + \cos^3(\varphi) D (-3x \dot{\varphi}^2 \sin(\varphi) + (m_b + 2m_{y1}) v_1 + v_2 D) \\
&\quad - \cos^4(\varphi) D (2\dot{\varphi} \dot{x} + 2x v_2 - 2m_x v_3 \sin(\varphi)) \\
&\quad + \cos^5(\varphi) (v_2 (x^2 + J_b) + 2x \dot{\varphi} \dot{x} + m_x (2D v_1 - x v_3 \sin(\varphi))) \\
u_{[2]} &= \frac{-1}{2Dk_m \cos^3(\varphi)} (D^2 \dot{\varphi}^2 \sin(\varphi) (8m_{y2} + 2m_b) + D^2 v_2 \cos(\varphi) (4m_{y2} + m_b) \\
&\quad + D \sin(\varphi) \cos^2(\varphi) (-m_b v_3 + \dot{\varphi}^2 D - 2v_3 m_{y2}) - \\
&\quad D \cos^2(\varphi) (\dot{\varphi} \dot{x} (2m_b + 4m_{y2}) + x v_2 (2m_{y2} + m_b)) \\
&\quad - D \cos^3(\varphi) (v_1 (m_b + 2m_{y2}) v_1 + x \sin(\varphi) \dot{\varphi}^2 - v_2 D) \\
&\quad - D \cos^4(\varphi) (2\dot{\varphi} \dot{x} + 2x v_2) \\
&\quad + \cos^5(\varphi) (v_2 (x^2 + J_b) + x (\dot{\varphi} \dot{x} - m_x \sin(\varphi) v_3)) \\
&\quad - m_x x v_1 \cos^6(\varphi) \\
u_{[3]} &= \frac{1}{k_m \cos(\varphi)} (-\cos(\varphi) (\dot{\varphi}^2 x + m_x \sin(\varphi) v_1) + m_x \cos^2(\varphi) v_3 + D \dot{\varphi}^2) \quad (\text{B.9})
\end{aligned}$$

## Appendix C

# IO linearization using matrix/vector calculation

As seen in chapter 2 the system outputs are defined as:

$$\underline{y} = \begin{bmatrix} y + D \tan(\varphi) - x \sin(\varphi) \\ \varphi \\ -D + x \cos(\varphi) \end{bmatrix}. \quad (\text{C.1})$$

The time derivatives of these outputs are:

$$\dot{\underline{y}} = \frac{\partial \underline{y}}{\partial \underline{q}} \dot{\underline{q}} \quad (\text{C.2})$$

The second time derivative of these outputs can be calculated using:

$$\ddot{\underline{y}} = \begin{bmatrix} \frac{\partial \dot{\underline{y}}}{\partial \underline{q}} & \frac{\partial \dot{\underline{y}}}{\partial \dot{\underline{q}}} \end{bmatrix} \begin{bmatrix} \dot{\underline{q}} \\ \ddot{\underline{q}} \end{bmatrix}. \quad (\text{C.3})$$

Substitution of the equations of motion (3.2) in (C.3) yields:

$$\ddot{\underline{y}} = \begin{bmatrix} \frac{\partial \dot{\underline{y}}}{\partial \underline{q}} & \frac{\partial \dot{\underline{y}}}{\partial \dot{\underline{q}}} \end{bmatrix} \begin{bmatrix} -M(\underline{q})^{-1}H(\underline{q}, \dot{\underline{q}}) + M(\underline{q})^{-1}B(\underline{q})\underline{u} \end{bmatrix}, \quad (\text{C.4})$$

which can be simplified to

$$\ddot{\underline{y}} = \frac{\partial \dot{\underline{y}}}{\partial \underline{q}} \dot{\underline{q}} + \frac{\partial \dot{\underline{y}}}{\partial \dot{\underline{q}}} M^{-1}(B\underline{u} - H). \quad (\text{C.5})$$

When the state feedback control law  $\underline{u}$  is defined to be

$$\underline{u} = B^{-1} \left( H - M \left( \frac{\partial \dot{\underline{y}}}{\partial \underline{q}} \right)^{-1} \left( \frac{\partial \dot{\underline{y}}}{\partial \dot{\underline{q}}} \right) \dot{\underline{q}} + M \left( \frac{\partial \dot{\underline{y}}}{\partial \dot{\underline{q}}} \right)^{-1} \underline{v} \right) \quad (\text{C.6})$$

then (C.5) yields the closed loop, decoupled system:

$$\underline{\dot{y}} = \underline{v} \quad (\text{C.7})$$

Finally the state feedback control law C.6 can be written in the form

$$\underline{u} = B^{-1}M \left( \frac{\partial \underline{y}}{\partial \underline{\dot{q}}} \right)^{-1} \left( \underline{v} - \left( \left( \frac{\partial \underline{y}}{\partial \underline{q}} \right) \underline{\dot{q}} - \left( \frac{\partial \underline{y}}{\partial \underline{\dot{q}}} \right) M^{-1}H \right) \right) \quad (\text{C.8})$$

which corresponds to (3.8). From this result it appears that the matrix  $A(\underline{q}, \underline{\dot{q}})$  and the vector  $N(\underline{q}, \underline{\dot{q}})$  can be written like

$$A(\underline{q}, \underline{\dot{q}}) = \frac{\partial \underline{y}}{\partial \underline{\dot{q}}} M^{-1} B \quad , \quad N(\underline{q}, \underline{\dot{q}}) = \left( \frac{\partial \underline{y}}{\partial \underline{q}} \right) \underline{\dot{q}} - \left( \frac{\partial \underline{y}}{\partial \underline{\dot{q}}} \right) M^{-1} H. \quad (\text{C.9})$$

## Appendix D

# Experiment with feedforward amplification

In this appendix the results are shown for the experiment with amplification of the feedforward. When introducing  $k_y$  and  $k_x$  as the amplification factors formula (4.6) can be written like:

$$\begin{bmatrix} v_1 \\ v_2 \\ v_3 \end{bmatrix} = \begin{bmatrix} k_y \ddot{Y}_d \\ 0 \\ k_x \ddot{X}_d \end{bmatrix} - a_1 \begin{bmatrix} \dot{e}_Y \\ \dot{\varphi} \\ \dot{e}_X \end{bmatrix} - a_0 \begin{bmatrix} e_Y \\ e_\varphi \\ e_X \end{bmatrix} \quad (\text{D.1})$$

The optimal value for  $k_y$  and  $k_x$  is experimentally determined and is of magnitude 2.3 and 5 respectively.

In the figures D.1,D.2 and D.3 the results are shown of the experiment, using the feedforward amplification. The in this experiment used pole placements and parameter values are the same as used in the experiment of chapter 5.4.

As one can see the tracking error, figure D.1, of the y and x trajectory is reduced with respect to the experiment in chapter 5.4. The acceleration dependency is also faded. It is noted that the magnitude and shape of the tracking error of the beam angle is unchanged. This can be explained by the non-changed zero feedforward of the beam angle.

The output of the tracking controller is globally the same but notice that the optimal feedforward signal, in figure D.2, matches the output signal. This means that the contribution of the tracking controller is decreased with respect to the feedforward. The change of the current signals, figure D.3, do not differ significantly from those in chapter 5.4 but this seem logical because of the small difference in position.

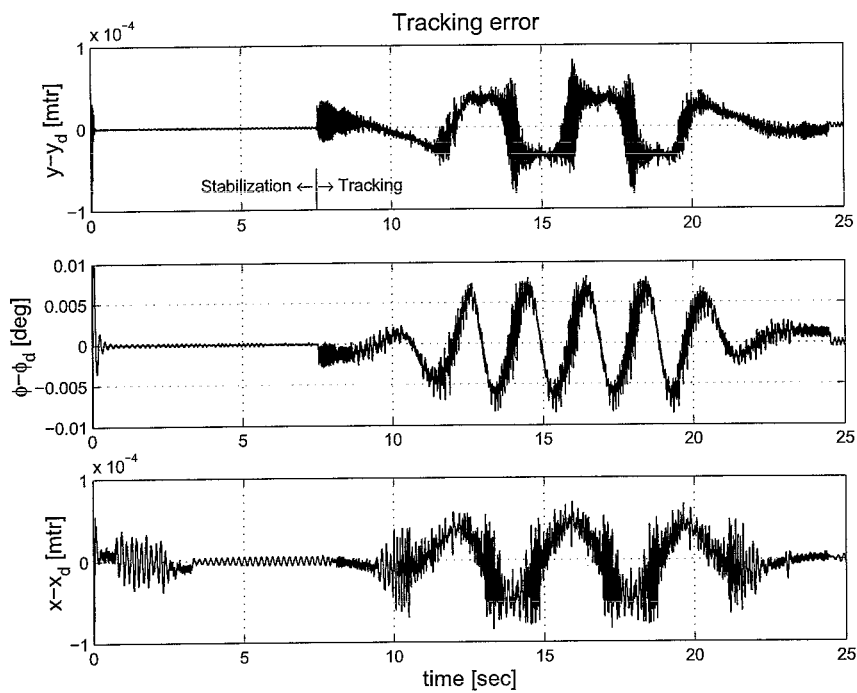


Figure D.1: Experiment using feedforward amplification: Tracking error

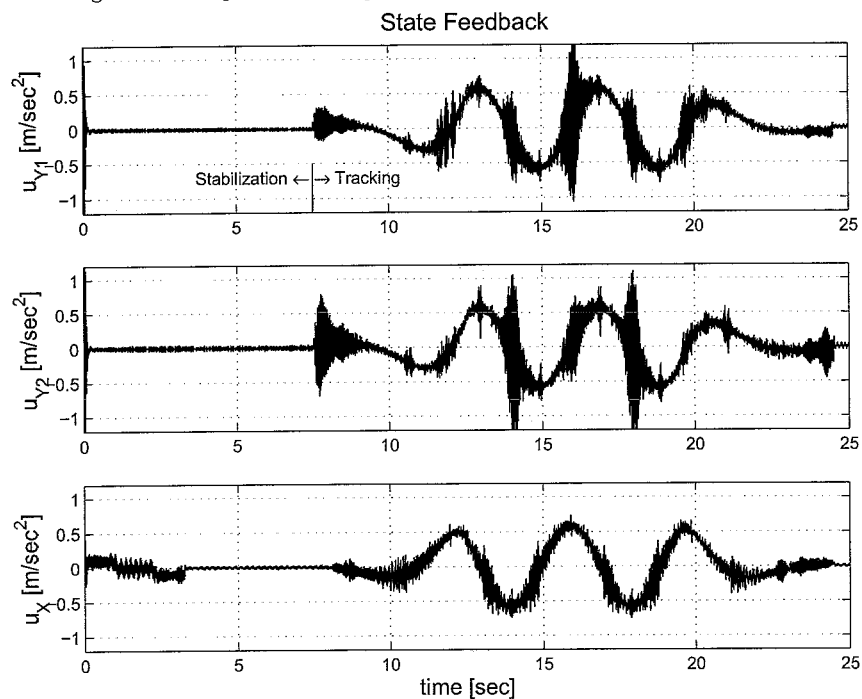
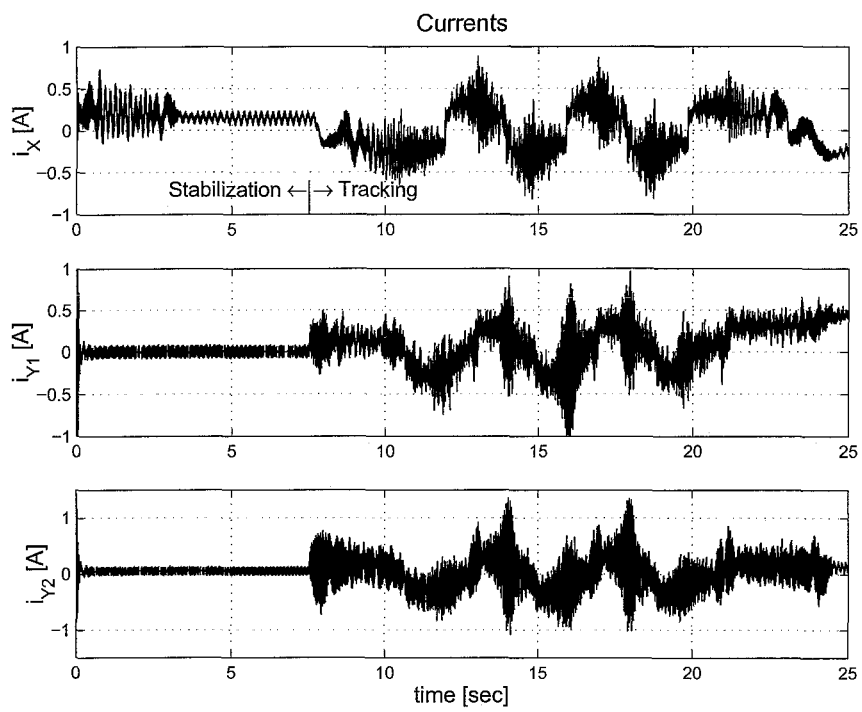


Figure D.2: Experiment using feedforward amplification: Tracking controller output [ $v_1; v_2; v_3$ ] (continuous) and the Feedforward (dashed)

Figure D.3: Experiment using feedforward amplification: Currents  $i_X$ ,  $i_{Y1}$  and  $i_{Y2}$

## Appendix E

# Programs used for the simulation and experiment

The programs used for the simulation and experiment are stored on the personal computer of the H-drive and on a CD-rom which is added to this report. The programs are provided with comments and short instructions.

The CD-rom contains also the  $\text{\LaTeX}$  and Adobe pdf version of this report and the presentation.

# Bibliography

- [1] N.P.I. Aneke. *Control of underactuated mechanical systems*. PhD thesis, Technische Universiteit Eindhoven, 2003.
- [2] S.G.M. Hendriks. Iterative learning control on the H-drive. Report internship, Eindhoven University of technology, December 2000.
- [3] K. Kosuge. *Virtual internal model following control of robot arms*. 1987. Proceedings of the *IEEE international conference on Robotics and automation*.
- [4] H.A. Pastink. Input output linearization on the underactuated H-drive. Report internship, Eindhoven University of technology, August 2003.
- [5] S. Sastry. *Nonlinear systems - Analysis, stability and control*. Springer Verlag, New York, 1999.
- [6] A van der Voort. LPV control based on a pick and place unit. Masters thesis, Eindhoven University of technology, Eindhoven, May 2002.
- [7] N. v.d. Wouw. *Multibody dynamics*. Technische Universiteit Eindhoven, Eindhoven, 2002.